

# Mixed-valence state approaching the single-impurity limit in La-substituted $\text{SmB}_6$

M. Zonno,<sup>1,2,3,\*</sup> M. Michiardi,<sup>1,2,4</sup> F. Boschini,<sup>2,5</sup> G. Levy,<sup>1,2</sup> K. Volkaert,<sup>6</sup> D. Curcio,<sup>6</sup> M. Bianchi,<sup>6</sup> P. F. S. Rosa,<sup>7</sup> Z. Fisk,<sup>8</sup> Ph. Hofmann,<sup>6</sup> I. S. Elfimov,<sup>1,2</sup> R. J. Green,<sup>9,2</sup> G. A. Sawatzky,<sup>1,2</sup> and A. Damascelli<sup>1,2,†</sup>

<sup>1</sup>*Department of Physics & Astronomy, University of British Columbia, Vancouver, BC V6T 1Z1, Canada*

<sup>2</sup>*Quantum Matter Institute, University of British Columbia, Vancouver, BC V6T 1Z1, Canada*

<sup>3</sup>*Canadian Light Source, Saskatoon, SK S7N 2V3, Canada*

<sup>4</sup>*Max Planck Institute for Chemical Physics of Solids, Nöthnitzer Straße 40, Dresden 01187, Germany*

<sup>5</sup>*Centre Énergie Matériaux Télécommunications Institut National de la Recherche Scientifique, Varennes, QC J3X 1S2, Canada*

<sup>6</sup>*Department of Physics and Astronomy, Interdisciplinary Nanoscience Center, Aarhus University, 8000 Aarhus C, Denmark*

<sup>7</sup>*Los Alamos National Laboratory, Los Alamos, New Mexico 87545, USA*

<sup>8</sup>*Department of Physics and Astronomy, University of California, Irvine, California 92697, USA*

<sup>9</sup>*Department of Physics & Engineering Physics, University of Saskatchewan, Saskatoon, SK S7N 5E2, Canada*

One of the most intriguing aspects of  $f$ -electron systems is their homogeneous mixed valence (MV) behavior. Despite extensive efforts, a fundamental aspect which remains unsettled is the determination of the limiting cases for which MV emerges, as highlighted by Haldane's theoretical proposal of the occurrence of a MV state for a single  $f$ -type impurity in a Fermi sea of  $d$ -electrons [1]. Here we address this open question for  $\text{SmB}_6$ , a prototypical system characterized by the interplay between two nearly-degenerate  $\text{Sm}^{2+}$  and  $\text{Sm}^{3+}$  configurations. By combining La substitution with angle-resolved photoemission (ARPES) and x-ray absorption spectroscopy (XAS), we track the evolution of the mean Sm valence for the  $f$ -shell,  $v_{Sm}$ , in the  $\text{Sm}_x\text{La}_{1-x}\text{B}_6$  series. Upon substitution of Sm ions by trivalent  $\text{La}^{3+}$ , we observe a linear decrease of valence fluctuations to an almost complete suppression at  $x=0.2$ , with  $v_{Sm} \sim 2$ ; surprisingly, by further reducing  $x$ , a re-entrant increase of  $v_{Sm}$  develops for  $x < 0.2$ , approaching a single-impurity-limit value of  $v_{imp} \sim 2.35$ . Such observation marks a stark deviation from a monotonic evolution of  $v_{Sm}$  across the entire series, as well as from the expectation of its convergence to an integer value for  $x \rightarrow 0$ . Our study suggests the realization of a *mixed-valence single-impurity state* in  $\text{Sm}_x\text{La}_{1-x}\text{B}_6$ , paving the way to further considerations on the concept of MV and its influence on the macroscopic properties of rare-earth compounds in the dilute-to-intermediate impurity regime.

Strong many-body interactions play a critical role in shaping the electronic, magnetic, and even mechanical properties of quantum materials. In compounds containing rare-earth or actinide elements, electron correlations originate from the localized and partially filled  $f$ -electron shells. The resulting entanglement of the relevant degrees of freedom – orbital, spin, charge, and lattice – gives rise to a plethora of novel phenomena in such materials, including superconductivity [2, 3], spin and charge order [4], quantum criticality [5], heavy fermion behavior [6, 7], Kondo physics [8], and mixed-valence behaviour [9, 10]. In particular, mixed valence (MV) is a fascinating phenomenon observed in a wide range of rare-earth compounds [9, 11–14], yet a full microscopic understanding of its limits remains elusive. MV is defined by the presence of a given rare-earth element exhibiting more than one electronic occupation for the  $f$  shell, and occurs when the total energy of these states are nearly degenerate [15]. Within the whole class of MV compounds, an important distinction arises between inhomogeneous and homogeneous MV scenarios. While in the former case ions with differing  $f$  occupation values reside on inequivalent crystallographic sites, in the latter all rare-earth ions retain the same non-integer  $f$  valence at each site [16, 17]. Here,

we focus on the case of homogeneous MV – also referred to as intermediate valence in the literature [16] –, to explore the parameter space in which such MV behaviour emerges. In fact, an early theoretical work by Haldane speculated the potential occurrence of a MV state even for a single  $f$ -type impurity in a Fermi sea of  $d$ -electrons [1], stimulating the debate on whether: (i) the MV concept can be extended down to the single-impurity limit; and (ii) if it can actually be observed experimentally.

In this work, we address these questions by investigating the crossover of a MV electronic ground state from a periodic  $f$ -electron lattice to a very dilute  $f$ -impurity system. We focus on the prototypical homogeneous mixed-valence system  $\text{SmB}_6$ , wherein the interplay between two nearly-degenerate  $f$ -shell valence configurations of the Sm ions profoundly shapes its electronic structure and macroscopic properties. While it has been shown that temperature and pressure may be exploited as external perturbations to tune the intermediate valence of the Sm ions [18–24], we base our experimental strategy on elemental substitution on the rare-earth site. This approach provides a powerful chemical control parameter acting directly on the occupation of the  $f$ -states, allowing the precise tracking of the mean Sm valence across different concentration regimes.

To this end, we employ trivalent La ions as substituent in the  $\text{Sm}_x\text{La}_{1-x}\text{B}_6$  hexaboride series. Although all the compounds of the series share the same CsCl-type crystal structure, the two end members exhibit very different

\* marta.zonno@lightsources.ca

† damascelli@physics.ubc.ca

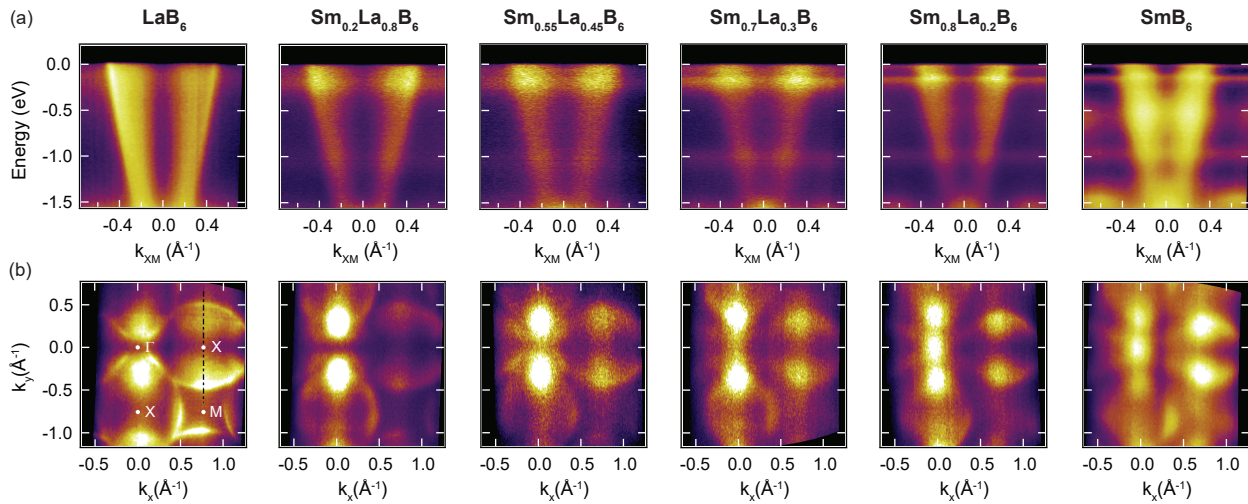


FIG. 1. ARPES spectra of  $\text{Sm}_x\text{La}_{1-x}\text{B}_6$ . (a) ARPES spectra along the  $\overline{XM}$  high-symmetry direction of the Brillouin zone [black dashed line in panel (b), left] for  $x = [0, 0.2, 0.55, 0.7, 0.8, 1]$ . (b) ARPES iso-energy contours close to  $E_F$  for the same samples shown in (a); the integration window in energy is 15 meV about  $E_F$ . All data were acquired at 10 K with  $h\nu = 21.2$  eV.

physics.  $\text{LaB}_6$  ( $x=0$ ) is metallic owing to the partially occupied La-5d band and the lack of 4f electrons. In contrast, the precise nature of the ground state of  $\text{SmB}_6$  ( $x=1$ ) still remains an open question. Exhibiting a resistivity plateau at low temperature [25], it has been theoretically proposed as realization of a topological Kondo insulator [26, 27], and various experimental studies have later discussed the possible presence and nature of in-gap electronic states [28–37], as well as controversial reports of quantum oscillations [38–40]. Even though a clear answer has yet to emerge, a fundamental aspect characterizing the physics of  $\text{SmB}_6$  is undoubtedly the nearly-complete admixture of the two possible Sm ions valence configurations  $4f^6 5d^0$  and  $4f^5 5d^1$ , which in terms of the  $f$ -level occupation are generally referred to as  $\text{Sm}^{2+}$  and  $\text{Sm}^{3+}$ , respectively. This leads to a mean Sm valence for the  $f$  shell of +2.505 in  $\text{SmB}_6$  at low temperature [18, 19, 41], while the single  $d$  band is characterized by a strongly mixed B-Sm character.

Here, by studying the electronic structure of  $\text{SmB}_6$  upon La substitution by angle-resolved photoemission (ARPES) and x-ray absorption spectroscopy (XAS), we observe a non-monotonic evolution of the mean Sm valence. While the strong  $\text{Sm}^{2+}/\text{Sm}^{3+}$  admixture is quenched in the intermediate substitution regime, it resurges for vanishing Sm concentrations, with a persisting MV behavior extrapolating all the way to the single-impurity limit. These results suggest the emergence of the MV phenomenon even in this extreme dilute limit, and establish the key role of unconventional behaviour of  $f$ -electrons in defining the properties of rare-earth compounds also in such extreme regime.

We begin by showcasing the evolution of the electronic structure of  $\text{Sm}_x\text{La}_{1-x}\text{B}_6$ , upon La-Sm chemical substitution, as measured by ARPES. Figure 1a summarizes

the ARPES spectra acquired along the  $\overline{XM}$  direction (black dashed line in Fig. 1b, left) for  $x = [0, 0.2, 0.55, 0.7, 0.8, 1]$ . Common to all compounds, bulk electron-like pockets are centered at the X high-symmetry points of the Brillouin zone (BZ), forming elliptic iso-energy contours (see Fig. 1b). Being primarily associated with B-2p and rare-earth 5d electrons, their size is directly related to the valence of the rare-earth element in the material: for a full 3+ configuration the  $d$ -pocket is half filled and at its largest, while in a 2+ state the valence electrons only fall in the  $f$ -states and the  $d$ -pocket lays in the unoccupied part of the spectrum. This observation makes the study of the evolution of the bulk 5d pockets centered at X instrumental to track the possible valence fluctuations of the Sm ions in the  $\text{Sm}_x\text{La}_{1-x}\text{B}_6$  series. As  $x$  increases, non-dispersing 4f-states emerge in the spectra in Fig. 1a at 15 meV, 150 meV, and 1 eV, consistent with what was reported previously for pristine  $\text{SmB}_6$  [31, 33, 42]. Concurrently, the size of the X-pockets in Fig. 1b progressively decreases upon increasing  $x$ , as expected from the removal of trivalent La ions which contribute to the occupation of the 5d-band.

However, we note that the observed behaviour departs from a constant-rate reduction, with the change in the ARPES dispersion being more pronounced for  $x \leq 0.55$  than for higher Sm concentrations. This progression is showcased by the evolution of the 5d-band dispersion extracted as a function of  $x$  along the  $\overline{\Gamma X}$  and  $\overline{XM}$  high-symmetry directions shown in Fig. 2a. In order to quantitatively assess this variation and thus establish a direct relation between the ARPES dispersion and the fractional percentage of  $\text{Sm}^{2+}$  and  $\text{Sm}^{3+}$  present in the system, we must convert the size of the X-pocket contours as extracted from the ARPES data into the pocket's occupation  $n^{5d}$ . This is done via application of the Luttinger's

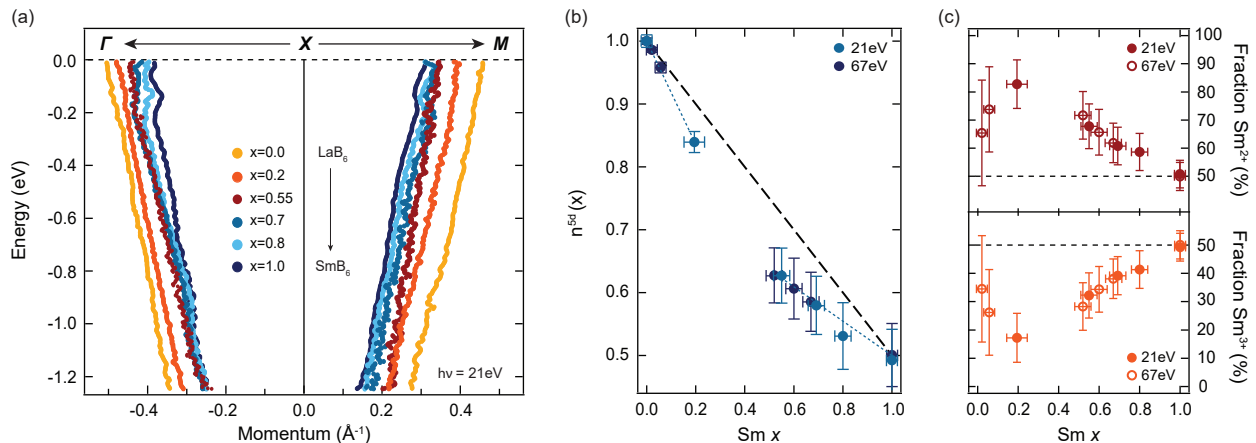


FIG. 2. Extracting the Sm valence from the ARPES dispersion. (a) Evolution of the X-pocket dispersion along  $\overline{\Gamma X}$  and  $\overline{XM}$  directions for  $x = [0, 0.2, 0.55, 0.7, 0.8, 1]$ , as extracted from the ARPES spectra in Fig. 1. (b) Electronic occupation number of the X-pocket,  $n_{5d}(x)$ , for different  $\text{Sm}_x\text{La}_{1-x}\text{B}_6$  compounds. Data points were obtained from ARPES spectra acquired with 21.2 eV and 67 eV. The dashed black line illustrates the case of a constant 1:1 ratio of  $\text{Sm}^{2+}:\text{Sm}^{3+}$  across the series; this is computed from the general expression  $n_{5d} = [1 - x * a / (a + b)]$ , where  $a$  and  $b$  are the fractional percentage of  $\text{Sm}^{2+}$  and  $\text{Sm}^{3+}$ , which reduces to  $n_{1:1}^{5d} = 1 - x/2$  in the case of  $a = b$ . (c) Calculated fractional percentage of  $\text{Sm}^{2+}$  (top) and  $\text{Sm}^{3+}$  (bottom) by using Eq. 1 for the different compounds measured by ARPES.

theorem, which directly relates the volume enclosed by a material's Fermi surface to the electron density [43, 44]. Here we emphasize that the bare X-pocket dispersion in the  $\text{Sm}_x\text{La}_{1-x}\text{B}_6$  series can be described to a first approximation by the same effective mass as observed for  $\text{LaB}_6$ , with the only Fermi momentum  $k_F^{5d}$  changing to accommodate for the varying electronic occupation. This assumption is supported by the ARPES dispersions shown in Fig. 2a, and facilitates a direct comparison among different compounds in the series.

Figure 2b displays the values of  $n_{5d}(x)$  as extracted via Luttinger's theorem from the ARPES spectra acquired with 21.2 eV and 67 eV probe energy (the latter associated to the bulk  $\Gamma$  high-symmetry point; see Supplementary Materials). The values were obtained by calculating the total enclosed volume of the X-pockets based on the collected ARPES while relying on the cubic crystal symmetry, and by taking into account the reported variation of the lattice parameter in the  $\text{Sm}_x\text{La}_{1-x}\text{B}_6$  series [45, 46]. For  $\text{LaB}_6$  ( $x = 0$ ), the pockets enclose  $\sim 50\%$  of the bulk cubic BZ, corresponding to having 1 electron  $n_{5d} = 1$ . At the other end of the series, in  $\text{SmB}_6$  ( $x = 1$ ) only a quarter of the cubic BZ is filled by the X-pockets, yielding  $n_{5d} = 0.5$ . These results are fully consistent with the metallic ground state observed in  $\text{LaB}_6$  and the reported valence of  $+2.505$  of Sm ions in  $\text{SmB}_6$ , thus validating our analysis. By applying the same approach to the intermediate compounds of the series, we find that  $n_{5d}(x)$  clearly deviates from the linear reduction expected in the case of a constant 1:1 ratio of  $\text{Sm}^{2+}:\text{Sm}^{3+}$ , represented in Fig. 2b by the black dashed line. To better quantify the evolution, we compute the fractional percentage of  $\text{Sm}^{2+}$  and  $\text{Sm}^{3+}$  from  $n_{5d}(x)$ , as follows (nor-

malized over the total amount of Sm in the system,  $x$ ):

$$\begin{aligned} \text{Fraction Sm}^{2+} (\%) &= \frac{1 - n_{5d}(x)}{x} \\ \text{Fraction Sm}^{3+} (\%) &= 1 + \frac{n_{5d}(x) - 1}{x} \end{aligned} \quad (1)$$

The resulting values are presented in Fig. 2c. As  $x$  decreases from 1, the amount of  $\text{Sm}^{2+}$  gradually increases upon reaching a maximum of  $\sim 85\%$  at  $x = 0.2$ , followed by a re-entrant reduction at even lower Sm concentrations. Despite the uncertainties associated with probing minimal modifications of the X-pocket ARPES dispersion for concentrations smaller than 0.1 (as reflected in the large error bars in Fig. 2c), our ARPES results suggest a clear distinction between the low ( $x \leq 0.2$ ) and high ( $x \geq 0.55$ ) Sm concentration regimes, along with a substantial variation of the  $\text{Sm}^{2+}:\text{Sm}^{3+}$  ratio across the  $\text{Sm}_x\text{La}_{1-x}\text{B}_6$  series.

In an effort to verify this scenario, especially on the low concentration regime, we complemented the ARPES data with a XAS study of the same  $\text{Sm}_x\text{La}_{1-x}\text{B}_6$  series. In particular, to achieve a higher bulk sensitivity and thus establish our results as an intrinsic bulk-property, we exploited partial and inverse partial fluorescence yield (PFY and IPFY), both defined by a probing depth of tens of nm. This allows one to circumvent some of the challenges characteristic of ARPES on  $\text{Sm}_x\text{La}_{1-x}\text{B}_6$ , such as cleaving and surface degradation. Furthermore, XAS has already been shown to be a powerful technique to explore the physics of MV systems, such as  $\text{SmB}_6$ : the absorption spectrum can be described to first approximation by the sum of two independent components, corresponding to  $\text{Sm}^{2+}$  and  $\text{Sm}^{3+}$  ions. By tuning the incident energy

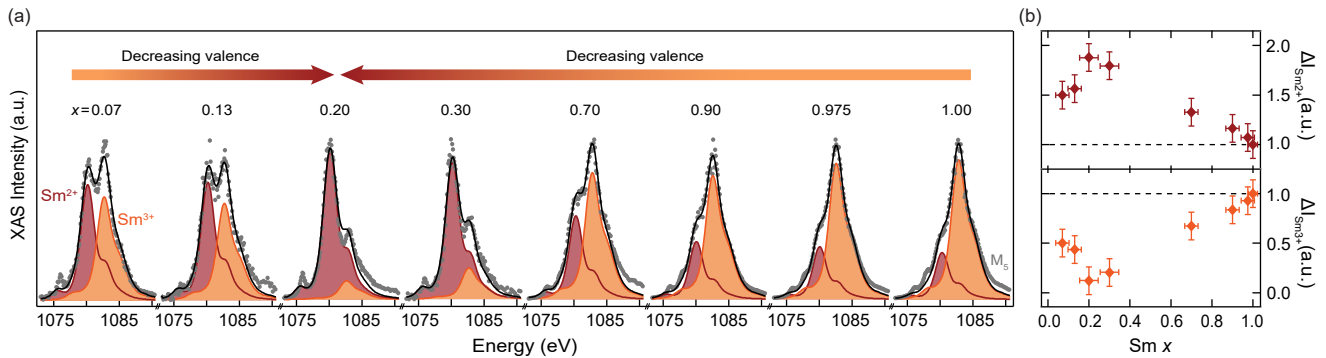


FIG. 3. XAS study of the  $\text{Sm}_x\text{La}_{1-x}\text{B}_6$  series. (a) Evolution of the XAS intensity at the Sm  $M_5$  edge for  $x = [0.07, 0.13, 0.2, 0.3, 0.7, 0.9, 0.975, 1]$ . The absorption profiles have been extracted at 640 eV (La fluorescence line) of IPFY spectra for  $x \leq 0.3$ , and at 850 eV (Sm fluorescence line) of PFY spectra for  $x > 0.3$ . The total XAS spectral weight is fit by the sum of two independent components associated to  $\text{Sm}^{2+}$  and  $\text{Sm}^{3+}$  ions (red and orange, respectively). (b) Intensity evolution of the  $\text{Sm}^{2+}$  (top) and  $\text{Sm}^{3+}$  (bottom) components normalized to the  $x = 1$  case. All data were taken at a base temperature of 20 K.

across the Sm  $M_4$  and  $M_5$  edges (i.e. exciting  $3d$  core electrons into  $4f$  orbitals), each XAS spectrum can be mapped into a specific  $\text{Sm}^{2+}:\text{Sm}^{3+}$  ratio, providing us with a tool to directly determine the mean Sm valence in the  $\text{Sm}_x\text{La}_{1-x}\text{B}_6$  series.

In Fig. 3a we present the evolution of the XAS intensity at the Sm  $M_5$  edge for  $x = [0.07, 0.13, 0.2, 0.3, 0.7, 0.9, 0.975, 1]$ , along with a weighted sum fit of the  $\text{Sm}^{2+}$  and  $\text{Sm}^{3+}$  components (red and orange, respectively). While for high  $x$  the  $\text{Sm}^{3+}$  component dominates, its contribution dramatically reduces at  $x = 0.2$ . However, upon further decrease of  $x$ , a clear inversion in the progression of the XAS spectra is observed, as the  $\text{Sm}^{3+}$  component strengthens again for  $x \leq 0.2$ . Such behaviour is highlighted by the intensity variation of the two components displayed in Fig. 3b (normalized to the  $x = 1$  values) and is fully consistent with the evolution of the fractional percentages of  $\text{Sm}^{2+}$  and  $\text{Sm}^{3+}$  obtained from ARPES, thus confirming the two-regime scenario already suggested in Fig. 2. In particular, the  $\text{Sm}^{2+}$  contribution peaks nearly doubling at  $x = 0.2$ , corresponding to an increment of  $\text{Sm}^{2+}$  ions in the system as large as  $\sim 90\%$  with respect to the pure  $\text{SmB}_6$  case. We remark that such significant increase of  $\text{Sm}^{2+}$  sets apart from what reported on pure  $\text{SmB}_6$  by employing high temperature and high pressure, with both perturbations causing an increase of the mean Sm valence towards  $+3$  [18–24]. Please also note that the deviation from an almost 1:1 ratio of the  $\text{Sm}^{2+}:\text{Sm}^{3+}$  peaks expected at  $x = 1$  may reflect a difference in the relative cross-sections of the two Sm components at the energies the XAS measurements were performed: while not affecting the qualitative evolution of the intensities shown in Fig. 3b, it is taken into account for computing the mean Sm valence (see Supplementary).

In Fig. 2 and 3 we showed that both ARPES and XAS measurements of the  $\text{Sm}_x\text{La}_{1-x}\text{B}_6$  series display a progression from an evenly  $\text{Sm}^{2+}/\text{Sm}^{3+}$  regime into a predominant presence of  $\text{Sm}^{2+}$  as  $x$  decreases. This result is consistent with the observation of the average Sm va-

lence tending towards  $+2$  upon trivalent ion substitution (such as  $\text{La}^{3+}$  or  $\text{Y}^{3+}$ ) reported in early studies [45, 46]. Furthermore, recent transport studies on La-substituted  $\text{SmB}_6$  have reported the complete closure of the  $d$ - $f$  hybridization gap, and the consequent emergence of a metallic-like behaviour, for La concentrations higher than 25% (here  $x \leq 0.75$ ) [47, 48], corroborating the substantial increase of  $\text{Sm}^{2+}$  in the system observed in this work. However, according to these arguments one may expect the valence fluctuations to be quenched at zero doping, i.e.  $v_{Sm} \rightarrow +2$  for  $x \rightarrow 0$ , in stark contrast with the clear suppression detected at  $x = 0.2$ , and followed by the sudden overturn for even lower  $x$ .

Here we present a basic phenomenological model for  $v_{Sm}$  in the  $\text{Sm}_x\text{La}_{1-x}\text{B}_6$  series based on the two distinct regimes observed experimentally. On one hand, for high  $x$  we mimic the convergence towards  $+2$  upon La substitution by fitting the experimental data for  $x \geq 0.2$  with a linear fit,  $V_0(x)$  [orange line in Fig. 4a]. On the other hand, to provide a phenomenological description of the increase of  $v_{Sm}$  detected at low  $x$  (i.e.  $x < 0.2$ ), we refer to an early work by Haldane which examines the dilute limit of a single rare-earth  $f$  impurity in a  $d$ -band metal [1]. The theoretical derivation is based on the addition to the Anderson-model Hamiltonian of a screening term, which describes the onsite interaction between the impurity  $f$ -orbitals and the  $d$ -orbitals. If this extra  $f$ - $d$  interaction is reasonably larger than the standard inter-site hybridization term, the model contemplates a stabilization of the  $f$ -electrons fluctuations, enabling *the single impurity to be in a mixed-valent state*. Although we recognize that the realization of such scenario would require a critical balance of  $f$  and  $d$  interplay, the system described in Haldane’s work retains a qualitative similarity with  $\text{Sm}_x\text{La}_{1-x}\text{B}_6$  for  $x \ll 1$ , where the Sm ions can be described as impurities in the  $d$ -band metal  $\text{LaB}_6$ .

This observation stimulates us to consider the possibility of additional contributions to  $v_{Sm}$  stemming from Sm ions acting as single impurities with a specific fixed



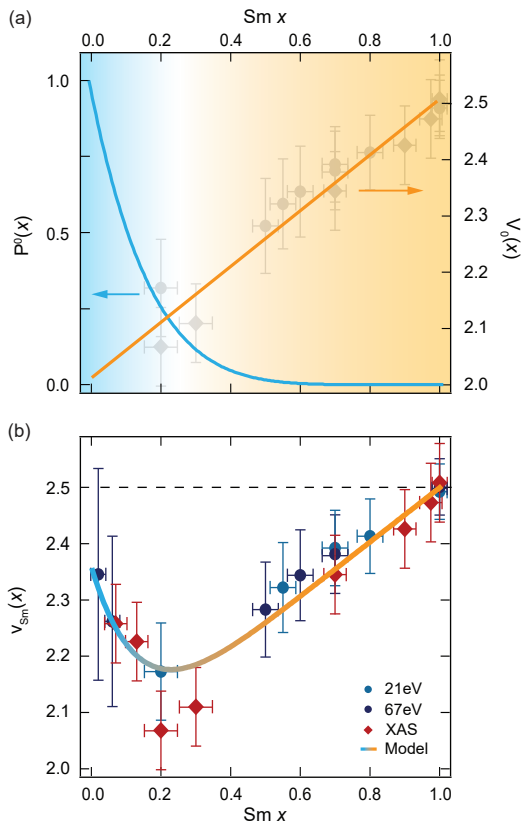


FIG. 4. Simplified model for the description of  $v_{Sm}$  in the two different  $x$  regimes. (a) Light blue line: calculated probability for a Sm ions to have no other Sm as next-nearest-neighbours,  $P^0(x)$ . This function is used to define the fraction of Sm ions which acquires the impurity valence  $v_{imp} = 2.35$  at each  $x$ . Orange line: linear fit to the experimental  $v_{Sm}$  values for  $x \geq 0.2$  (grey data points),  $V_0(x)$ , capturing the decrease in the valence due to formation of  $Sm^{2+}$  upon La-substitution. (b) Comparison between the model of Eq.2 and the experimental values of  $v_{Sm}$  obtained from ARPES (light and dark blue circles, acquired with 21 eV and 67 eV, respectively) and XAS (red diamonds).

intermediate valence,  $v_{imp}$ . In this regard, we compute the probability as a function of  $x$  for a Sm ion to have no other Sm in the next-nearest-neighbour sites,  $P^0(x)$  [light blue line in Fig.4a]. This function is used to define in first approximation the fraction of Sm ions that exhibits an impurity valence  $v_{imp} = +2.35$ , as extrapolated from the experimental results in Figs. 2c-3b, at any given concentration  $x$ . We can then express the evolution of the Sm valence in the  $Sm_xLa_{1-x}B_6$  series as:

$$v_{model} = P^0(x) \cdot v_{imp} + [1 - P^0(x)] \cdot V_0(x) \quad . \quad (2)$$

Fig.4b compares the model of Eq. 2 with the experimental values of the average Sm valence obtained from ARPES (light and dark blue circles) and XAS (red diamonds), showing an overall good agreement. In particular, the inclusion of the emerging Sm impurity regime with fixed fractional valence is proven pivotal to capture the steep

increase of  $v_{Sm}$  experimentally observed for low  $x$ ; however, its contribution becomes negligible at high  $x$ , owing to the rapid decay of  $P^0(x)$  below 0.1 for  $x \geq 0.3$ .

As a final note, we emphasize that the model of Eq. 2 does not fully describe the nearly-complete suppression of  $Sm^{2+}/Sm^{3+}$  admixture detected at  $x = 0.2$ ; indeed additional investigations are needed to specifically address such deviation with the development of more refined theories. Nevertheless, our combined ARPES and XAS study provides evidence of the realization of a single-impurity MV state in the  $Sm_xLa_{1-x}B_6$  series. Our results may stimulate further theoretical and experimental considerations on the concept of mixed valence and its influence on the macroscopic electronic and transport properties of rare-earth compounds in the dilute-to-intermediate impurity regime.

## METHODS

High-quality single crystals of  $Sm_xLa_{1-x}B_6$  were grown by the aluminum flux method in a continuous Ar-purged vertical high-temperature tube furnace [28]. Post-growth characterization by scanning electron microscope and energy dispersive x-ray measurements for the actual Sm concentration was performed at the Center for Integrated Nanotechnologies, an Office of Science User Facility operated for the U.S. Department of Energy Office of Science. ARPES experiments were performed at the Stewart Blusson Quantum Matter Institute at UBC employing a photon energy of  $h\nu = 21.2$  eV, at a base pressure  $< 3 \cdot 10^{-11}$  Torr and base temperature of 10 K. The electrons were collected using a SPECS Phoibos 150 hemispherical analyzer, with energy and momentum resolution of 25 meV and 0.02 Å, respectively. Additional ARPES measurements were carried out at the SGM3 endstation at the ASTRID2 synchrotron radiation facility [49], using a photon energy of  $h\nu = 67$  eV, with base temperature 35 K and energy resolution 35 meV. All samples were cleaved *in-situ* and measured along the (001) surface. XAS measurements were performed using the four-circle UHV diffractometer at the REIXS 10ID-2 beamline at the Canadian Light Source in Saskatoon [50], with base pressure and temperature of  $5 \cdot 10^{-10}$  Torr and 22 K, respectively.

## ACKNOWLEDGMENTS

This research was undertaken thanks in part to funding from the Max Planck-UBC-UTokyo Centre for Quantum Materials and the Canada First Research Excellence Fund, Quantum Materials and Future Technologies Program. This project is also funded by the Killam, Alfred P. Sloan, and Natural Sciences and Engineering Research Council of Canada's (NSERC's) Steacie Memorial Fellowships (A.D.); the Alexander von Humboldt Fellowship (A.D.); the Canada Research Chairs

Program (A.D.); NSERC, Canada Foundation for Innovation (CFI); the Department of National Defence (DND); British Columbia Knowledge Development Fund (BCKDF); and the CIFAR Quantum Materials Program. E.R. acknowledges support from the Swiss National Science Foundation (SNSF) grant no. P300P2 164649. Part of the research described in this work was performed at the Canadian Light Source, a national research facility of the University of Saskatchewan, which is supported by CFI, NSERC, the National Research Council (NRC),

the Canadian Institutes of Health Research (CIHR), the Government of Saskatchewan, and the University of Saskatchewan. The research carried out in Aarhus was supported by the Independent Research Fund Denmark (Grant No. 1026-00089B) and the VILLUM FONDEN via the Centre of Excellence for Dirac Materials (Grant No. 11744). Work at Los Alamos was performed under the auspices of the U.S. Department of Energy, Office of Basic Energy Sciences, Division of Materials Science and Engineering.

- 
- [1] F. D. M. Haldane, *Physical Review B* **15**, 2477 (1977).
- [2] N. D. Mathur, F. M. Grosche, S. R. Julian, I. R. Walker, D. M. Freye, R. K. W. Haselwimmer, and G. Lonzarich, *Nature* **394**, 39 (1998).
- [3] T. Moriya and K. Ueda, *Reports on Progress in Physics* **66**, 1299 (2003).
- [4] T. Hotta, *Reports on Progress in Physics* **69**, 2061 (2006).
- [5] P. Gegenwart, Q. Si, and F. Steglich, *Nature Physics* **4**, 186 (2008).
- [6] Z. Fisk, D. W. Hess, C. J. Pethick, D. Pines, J. L. Smith, J. D. Thompson, and J. O. Willis, *Science* **239**, 33 (1988).
- [7] P. Coleman, arXiv preprint arXiv:1509.05769 (2015).
- [8] J. Kondo, *Progress of Theoretical Physics* **32**, 37 (1964).
- [9] C. M. Varma, *Reviews of Modern Physics* **48**, 219 (1976).
- [10] P. Day, *Molecules Into Materials: Case Studies in Materials Chemistry-Mixed Valency, Magnetism and Superconductivity* (World Scientific, 2007).
- [11] J. M. Lawrence, P. S. Riseborough, and R. D. Parks, *Reports on Progress in Physics* **44**, 1 (1981).
- [12] K. Buschow, *Reports on Progress in Physics* **42**, 1373 (1979).
- [13] J. M. D. Coey, M. Viret, and S. Von Molnar, *Advances in Physics* **48**, 167 (1999).
- [14] R. Parks, *Valence instabilities and related narrow-band phenomena* (Springer Science & Business Media, 2012).
- [15] P. W. Anderson, Present status of theory: 1/N approach, in *Moment Formation In Solids*, edited by W. J. L. Buyers (Springer US, 1984) pp. 313–326.
- [16] P. S. Riseborough and J. M. Lawrence, *Reports on Progress in Physics* **79**, 084501 (2016).
- [17] P. S. Riseborough, *Advances in Physics* **49**, 257 (2000).
- [18] J.-M. Tarascon, Y. Isikawa, J. Chevalier, B. and Etourneau, P. Hagenmuller, and M. Kasaya, *Journal de Physique* **41**, 1141 (1980).
- [19] M. Mizumaki, S. Tsutsui, and F. Iga, in *Journal of Physics: Conference Series*, Vol. 176 (IOP Publishing, 2009) p. 012034.
- [20] N. P. Butch, J. Paglione, P. Chow, Y. Xiao, C. A. Marianetti, C. H. Booth, and J. R. Jeffries, *Physical Review Letters* **116**, 156401 (2016).
- [21] L. Sun and Q. Wu, *Reports on Progress in Physics* **79**, 084503 (2016).
- [22] J.-M. Lee, S.-C. Haw, S.-W. Chen, S.-A. Chen, H. Ishii, K.-D. Tsuei, N. Hiraoka, Y.-F. Liao, K.-T. Lu, and J.-M. Chen, *Dalton Transactions* **46**, 11664 (2017).
- [23] Y. Zhou, Q. Wu, P. F. Rosa, R. Yu, J. Guo, W. Yi, S. Zhang, Z. Wang, H. Wang, S. Cai, K. Yang, A. Li, Z. Jiang, S. Zhang, X. Wei, Y. Huang, P. Sun, Y. feng Yang, Z. Fisk, Q. Si, Z. Zhao, and L. Sun, *Science Bulletin* **62**, 1439 (2017).
- [24] N. Emi, T. Mito, N. Kawamura, M. Mizumaki, N. Ishimatsu, G. Pristáš, T. Kagayama, K. Shimizu, Y. Osanai, and F. Iga, *Physica B: Condensed Matter* **536**, 197 (2018).
- [25] A. Menth, E. Buehler, and T. H. Geballe, *Physical Review Letters* **22**, 295 (1969).
- [26] M. Dzero, K. Sun, V. Galitski, and P. Coleman, *Physical Review Letters* **104**, 106408 (2010).
- [27] M. Dzero, K. Sun, P. Coleman, and V. Galitski, *Physical Review B* **85**, 045130 (2012).
- [28] S. Wolgast, Ç. Kurdak, K. Sun, J. W. Allen, D.-J. Kim, and Z. Fisk, *Physical Review B* **88**, 180405 (2013).
- [29] X. Zhang, N. P. Butch, P. Syers, S. Ziemak, R. L. Greene, and J. Paglione, *Physical Review X* **3**, 011011 (2013).
- [30] D. J. Kim, S. Thomas, T. Grant, J. Botimer, Z. Fisk, and J. Xia, *Scientific Reports* **3**, 3150 (2013).
- [31] J. Jiang, S. Li, T. Zhang, Z. Sun, F. Chen, Z. R. Ye, M. Xu, Q. Q. Ge, S. Y. Tan, X. H. Niu, M. Xia, B. P. Xie, Y. F. Li, X. H. Chen, H. Wen, and D. L. Feng, *Nature Communications* **4**, 3010 (2013).
- [32] N. Xu, X. Shi, P. K. Biswas, C. E. Matt, R. S. Dhaka, Y. Huang, N. C. Plumb, M. Radović, J. H. Dil, E. Pomjakushina, K. Conder, A. Amato, Z. Salman, D. M. Paul, J. Mesot, H. Ding, and M. Shi, .
- [33] M. Neupane, N. Alidoust, S.-Y. Xu, T. Kondo, Y. Ishida, D.-J. Kim, C. Liu, I. Belopolski, Y. J. Jo, T.-R. Chang, H.-T. Jeng, T. Durakiewicz, L. Balicas, H. Lin, A. Bansil, S. Shin, Z. Fisk, and M. Z. Hasan, *Nature Communications* **4**, 2991 (2013).
- [34] E. Frantzeskakis, N. de Jong, B. Zwartsenberg, Y. K. Huang, Y. Pan, X. Zhang, J. X. Zhang, F. X. Zhang, L. H. Bao, O. Tegus, A. Varykhalov, A. de Visser, and M. S. Golden, *Physical Review X* **3**, 041024 (2013).
- [35] Z.-H. Zhu, A. Nicolaou, G. Levy, N. P. Butch, P. Syers, X. F. Wang, J. Paglione, G. A. Sawatzky, I. S. Elfimov, and A. Damascelli, *Physical Review Letters* **111**, 216402 (2013).
- [36] P. Hlawenka, K. Siemensmeyer, E. Weschke, A. Varykhalov, J. Sánchez-Barriga, N. Y. Shitsevalova, A. V. Dukhnenko, V. B. Filipov, S. Gabáni, K. Flachbart, O. Rader, and E. D. L. Rienks, *Nature Communications* **9**, 517 (2018).
- [37] C. M. Varma, *Physical Review B* **102**, 155145 (2020).
- [38] G. Li, Z. Xiang, F. Yu, T. Asaba, B. Lawson, P. Cai, C. Tinsman, A. Berkley, S. Wolgast, Y. S. Eo, D.-J. Kim, C. Kurdak, J. W. Allen, K. Sun, X. H. Chen, Y. Y. Wang, Z. Fisk, and L. Li, *Science* **346**, 1208 (2014).

- [39] B. S. Tan, Y.-T. Hsu, B. Zeng, M. C. Hatnean, N. Harrison, Z. Zhu, M. Hartstein, M. Kiourlappou, A. Srivastava, M. D. Johannes, T. P. Murphy, J.-H. Park, L. Balicas, G. G. Lonzarich, G. Balakrishnan, and S. E. Sebastian, *Science* **349**, 287 (2015).
- [40] S. M. Thomas, X. Ding, F. Ronning, V. Zapf, J. D. Thompson, Z. Fisk, J. Xia, and P. F. S. Rosa, *Phys. Rev. Lett.* **122**, 166401 (2019).
- [41] M. Sundermann, H. Yavaş, K. Chen, D. J. Kim, Z. Fisk, D. Kasinathan, M. W. Haverkort, P. Thalmeier, A. Severing, and L. H. Tjeng, *Physical Review Letters* **120**, 016402 (2018).
- [42] J. D. Denlinger, J. W. Allen, J.-S. Kang, K. Sun, B.-I. Min, D.-J. Kim, and Z. Fisk, in *Proceedings of the International Conference on Strongly Correlated Electron Systems (SCES2013)* (2014) p. 017038.
- [43] R. M. Martin, *Physical Review Letters* **48**, 362 (1982).
- [44] R. M. Martin, *Journal of Applied Physics* **53**, 2134 (1982).
- [45] M. Kasaya, J. M. Tarascon, and J. Etourneau, *Solid State Communications* **33**, 1005 (1980).
- [46] J.-M. Tarascon, Y. Isikawa, B. Chevalier, J. Etoumeau, P. Hagemuller, and M. Kasaya, *Journal de Physique* **41**, 1135 (1980).
- [47] B. Y. Kang, C.-H. Min, S. S. Lee, M. S. Song, K. K. Cho, and B. K. Cho, *Physical Review B* **94**, 165102 (2016).
- [48] S. Gabáni, M. Orendáč, G. Pristáš, E. Gažo, P. Diko, S. Piovarči, V. Glushkov, N. Sluchanko, A. Levchenko, N. Shitsevalova, and K. Flachbart, *Philosophical Magazine* **96**, 3274 (2016).
- [49] S. V. Hoffmann, C. Søndergaard, C. Schultz, Z. Li, and P. Hofmann, *Nuclear Instruments and Methods in Physics Research Section A: Accelerators, Spectrometers, Detectors and Associated Equipment* **523**, 441 (2004).
- [50] D. G. Hawthorn, F. He, L. Venema, H. Davis, A. J. Achkar, J. Zhang, R. Sutarto, H. Wadati, A. Radi, T. Wilson, G. Wright, K. M. Shen, J. Geck, H. Zhang, V. Novák, and G. A. Sawatzky, *Review of Scientific Instruments* **82**, 073104 (2011).